Journal of Superconductivity and Novel Magnetism (2019) 32:301–310
https://doi.org/10.1007/s10948-018-4707-7

ORIGINAL PAPER

Effect of Fe Substitution on the Physical Properties of $La_{0.62}Er_{0.05}Ba_{0.33}Mn_{1-x}Fe_xO_3$ ($x = 0.00$, 0.05 and 0.15)

Abassi Mounira[1]

Received: 15 March 2018 / Accepted: 24 April 2018 / Published online: 4 May 2018

Abstract

Morphology, magnetic and magnetocaloric properties of $La_{0.62}Er_{0.05}Ba_{0.33}Mn_{1-x}Fe_xO_3$ ($x = 0.00$, 0.05 and 0.15) were experimentally investigated. Solid-state reaction method was used in the preparation of the samples. The microstructure of the samples was determined by scanning electron microscopy (SEM). From the XRD study, it has been found that all samples are single-phased and crystallized in the rhombohedral structure with the R3-c space group. For $x = 0.05$ and 0.15, a steep drop of zero field-cooled (ZFC) magnetization at low temperature signifies the formation of cluster- or spin-glass state. This is caused by the competition between the ferromagnetic and antiferromagnetic interaction. A sensitive response to substituting Fe for Mn is observed in the magnetic and magnetocaloric properties. We found that Fe doping is powerful enough to reduce Curie temperature T_C and it brings about cluster glass behaviours. The magnetocaloric effect is calculated from the measurement of initial isothermal magnetization versus magnetic field at various temperatures. The maximum entropy change $\left|\Delta S_M^{\max}\right|$ reaches the highest values of 3.31, 3.12, and 2.57 J/kg K in magnetic field. However, the relative cooling power decreases with Fe content from $x = 227.44$ to 188.68 J/kg for $x = 0.00$ to $x = 0.15$ compositions, respectively.

Keywords Morphology · Manganite · Magnetic property · Magnetocaloric effect · Site B-substitution · Spin glass

1 Introduction

The manganites with general formula $RE_{1-x}AE_xMnO_3$, where RE and AE denote, respectively, trivalent rare earth and bivalent alkaline earth elements, have been widely studied during the last decade due to technological applications [1] in medicine [2–4], catalysis processes [5] and magnetic refrigeration [6, 7], for instance. In these perovskite compounds, the interplay between magnetism, charge ordering, and electronic transport have been studied in detail [8–11]. In particular, the metal-insulator transition near the Curie temperature in this class of material has been interpreted in terms of the double exchange (DE) model. But, there are some other mechanisms that have provided valuable insights into the colossal magnetoresistance (CMR) phenomenon in manganites, such as the anti-ferromagnetic super-exchange, Jahn-Teller effects and orbital and charge ordering [12, 13]. Other researches focused on perovskite manganites with a general formula $RE_{1-x}AE_xMnO_3$ after the observing large magnetocaloric effects (MCE) in these compounds [14–17]. Currently, MCE offers an alternative technology in refrigeration, with an enhanced efficiency but without environmental hazards [18–21]. The key in using magnetic refrigeration at room temperature is to seek the proper refrigerant materials which can produce a large entropy variation when it goes through a magnetization-demagnetization process. In terms of the crucial role of Mn site, it would be interesting and worthwhile to study the effects of Mn-site element substitution, which may provide clues for exploring novel MCE materials and concerning the mechanism of MCE. Within this framework, the effect of substituting trivalent ions such as Fe, Ni and Sc for Mn^{3+} ions in the B site on the ferromagnetic properties of these manganites has been studied [22–25]. It was experimentally found that any modification on the exchange interaction causes the pair-braking effect associated with a drastic reduction in Curie temperature T_C. However, differently from the common ionic substitution, Fe doping in manganites has a peculiar effect and is attracting more attention. This suggests that Fe substitution for Mn dilutes the DE mechanism and shows a typical spin glass

✉ Abassi Mounira
m.alabasi@su.edu.sa

[1] Physics Departement, Faculty of Education, Afif Governorate, Shaqra University, Shaqraa, Saudi Arabia

and insulating behaviours. The results of several authors who studied $Ln_{1-x}A_xMn_{1-y}Fe_yO_3$, Fe-doped manganites with y-x indicate the existence of an antiferromagnetic interaction between Fe and Mn ions [26–28]

In the present study, we investigate the structure, the magnetic properties and magnetocaloric effect of $La_{0.62}Er_{0.05}Ba_{0.33}Mn_{1-x}Fe_xO_3$ compounds, which can be a suitable candidate as a working substance in magnetic refrigeration at near room temperature. First, we explored the effect of Fe doping on the ground-state magnetic ordering properties of polycrystalline manganite $La_{0.62}Er_{0.05}Ba_{0.33}Mn_{1-x}Fe_xO_3$. Second, we considered important characteristics, such as large MCE values and being a ferromagnetic near and above room temperatures that would qualify the materials to be considered for practical applications. In this context, there are many studies on the hole-doped manganites, which vary the concentration of alkaline earth ions that affects the Mn^{3+}/Mn^{4+} ratio. Moreover, there are very few reports where a systematic analysis on magnetic and magnetocaloric properties is carried out especially on La-doped layered manganites.

2 Experimental Details

$La_{0.62}Er_{0.05}Ba_{0.33}Mn_{1-x}Fe_xO_3$ ($x = 0.00$, 0.05 and 0.15) were synthesized using the standard solid-state reaction method at high temperature. The detailed preparation procedure and basic physical properties are reported in ref. [29]. The magnetization measurements were carried out using a superconducting quantum interference device magnetometer in different magnetic fields at Neel institute.

3 Results and Discussions

3.1 Morphological Characterization and Structural Information

In order to check the existence of all the elements in the LEBMFO (0.00, 0.05 and 0.15) compounds, an energy-dispersive x-ray analysis was performed. An example of EDX spectra is represented in Fig. 1 for $x = 0.05$. This spectrum reveals the presence of all elements (La, Er, Ba, Mn, Fe and O), which confirms that there is no loss of any integrated element during sintering. The SEM micrographs are given in the insets of this figure for $x = 0.05$. We can see that the grains exhibit spheroid-like shapes and a good connectivity between each other. This facilitates the intrinsic behaviours because good current percolation between grains and the opening up of conduction channels do not block the ordering of the Mn spins. The typical cationic composition for the samples is represented in Table 1. The synthesized size is one of structural parameters which can be determined with the help of XRD data using the following mathematical relations [30]:

$$D_{SC} = \frac{k\lambda}{\beta \cos\theta} \quad (1)$$

where D_{SC} is the crystallite size, $k$is a constant and its value is 0.9, λ is the wave length of x-ray used (1.541 ?), θ is Bragg's angle and β is the full width at half maxima. Additionally, we can also calculate the grain size using a scanning electron microscopy (SEM). As shown in Table 2, the average grain size (D_{SC}) obtained from the XRD peaks using the Scherrer formula (1) is significantly smaller than

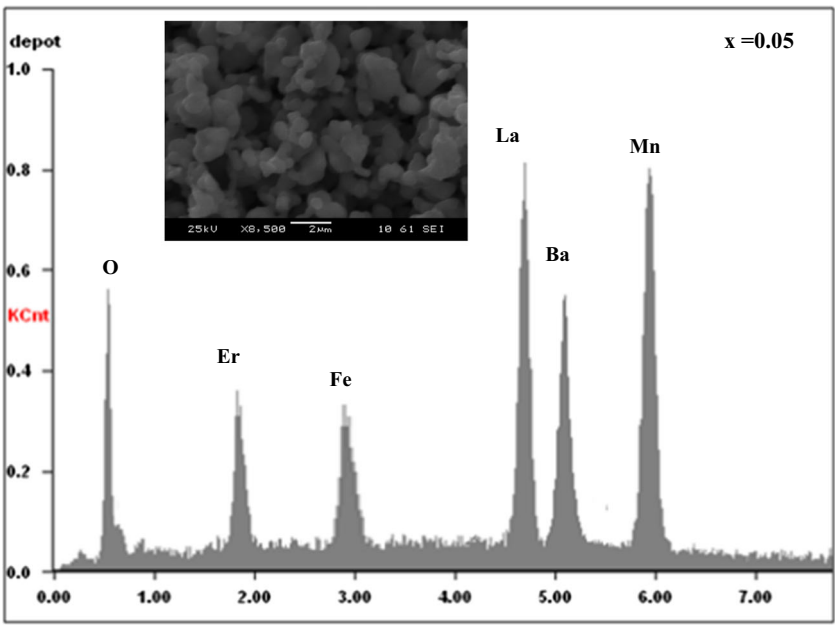

Fig. 1 Plot of EDX analysis of chemical species, the inset represents the scanning electron micrograph of $x = 0.05$

Table 1 Results of EDX analysis

Composition	Typical cationic composition from EDX					Nominal composition
	La	Er	Ba	Mn	Fe	
$x = 0.00$	0.619	0.052	0.329	1.008	–	$La_{0.62}Er_{0.05}Ba_{0.33}MnO_3$
$x = 0.05$	0.621	0.053	0.326	0.951	0.052	$La_{0.62}Er_{0.05}Ba_{0.33}Mn_{0.95}Fe_{0.05}O_3$
$x = 0.15$	0.624	0.052	0.324	0.842	0.158	$La_{0.62}Er_{0.05}Ba_{0.33}Mn_{0.85}Fe_{0.15}O_3$

the values determined by SEM, which indicates that each particle observed by SEM consists of several crystallized grains [31].

Furthermore, to find close values, we have used Williamson-Hall approach for deconvoluting size and strain contribution to the x-ray line broadening. According to this approach, the x-ray line broadening is a sum of the contribution from small crystallite size and the broadening caused by the lattice strain present in the material [32], i.e.

$$\beta = \beta_{\text{size}} + \beta_{\text{strain}} \tag{2}$$

where $\beta_{\text{size}} = \frac{k\lambda}{D\cos\theta}$ and $\beta_{\text{strain}} = 4\delta \tan g\theta$, where δ is strain $\frac{\Delta l}{l}$, so Eq. 2 becomes

$$\beta = \frac{k\lambda}{D\cos\theta} + 4\delta \tan g\theta \tag{3}$$

$$\beta\cos\theta = \frac{k\lambda}{D} + 4\delta \sin\theta \tag{4}$$

where 4δ is a measure of strain present in the lattice hence by plotting $\beta\cos\theta$ versus $4\sin\theta$, we can find the crystallite size from the intercept $(\frac{k\lambda}{D})$ of this line on the y-axis and the slope of the line gives the strain (δ). Figure 2 shows the strain measurements of all the samples. The strain measured from the slope increases with increasing Fe doping which indicates that strain increases as larger Fe ion accommodates in MnO_3 matrix. The variation in cation distribution on the rhombohedra sites produces compressive strain due to the variation of ionic sizes of the two cations. The crystallite size (D) and the strain (δ) are listed in Table 2. The crystallite size $(D) = 98$, 105 and 109 nm and the strain $(\delta) = 0.354$, 0.361 and 0.369 for $x = 0.00$, 0.05 and 0.15, respectively, are listed in Table 2. The crystallite size calculated in the present system using the William-Hall technique is larger than the crystallite size $(D_{\text{SC}}) = 160.7$, 164.12 and 170.32 nm for $x = 0.00$, 0.05 and 0.15, respectively, because the broadening effect due to strain is completely excluded in Debye-Sherrer technique [33].

Table 2 Different grain size (crystallite size D_{SC} from relation Debye-Scherrer, D_{MEB} using a scanning electron microscopy and D from Williamson-Hall)

	Samples		
	$x = 0.00$	$x = 0.05$	$x = 0.15$
D_{Sc} (nm)	160.7	164.12	170.32
D_{MEB} (nm)	475	480	485
D (nm)	100	105	109
Strain (δ)	0.354	0.361	0.369

3.2 Magnetic Behaviours

Figure 3a presents the magnetization curves as a function of temperature at zero field-cooled (ZFC) and field-cooled (FC) under an external magnetic field of 500 Oe for LEBMFO. As can be seen, all the LEBMFO samples undergo a transition from a ferromagnetic to a paramagnetic phase. It is clear that the FC curves do not coincide with the ZFC curves below T_C. But the curves FC and ZFC have a common part for the high temperature wherein the variation of magnetization with temperature is reversible and superposed. At low temperature, the behaviour is irreversible with a divergence between ZFC and FC. The magnetic moment gradually reduces. Such irreversibility in the M-T data for the FC and ZFC measurements was observed in several manganite systems and it was suggested that this irreversibility is possibly due to the canted nature of the spins or due to the random freezing of spins [34]. This can be seen clearly at low temperature for $x = 0.15$, which

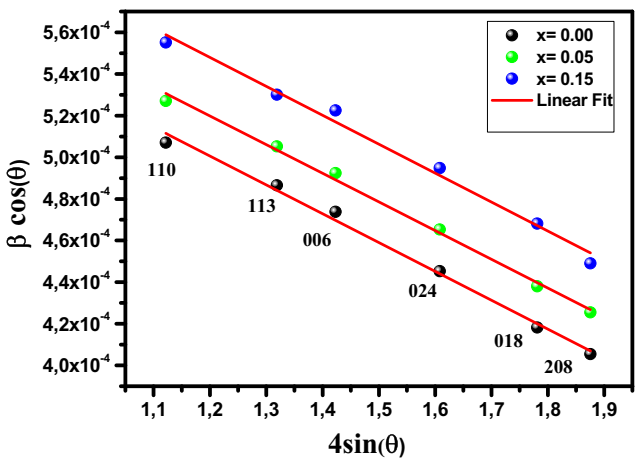

Fig. 2 Variation of strain graph for $La_{0.62}Er_{0.05}Ba_{0.33}Mn_{1-x}Fe_xO_3$ for ($x = 0.00$, 0.05 and 0.15) samples

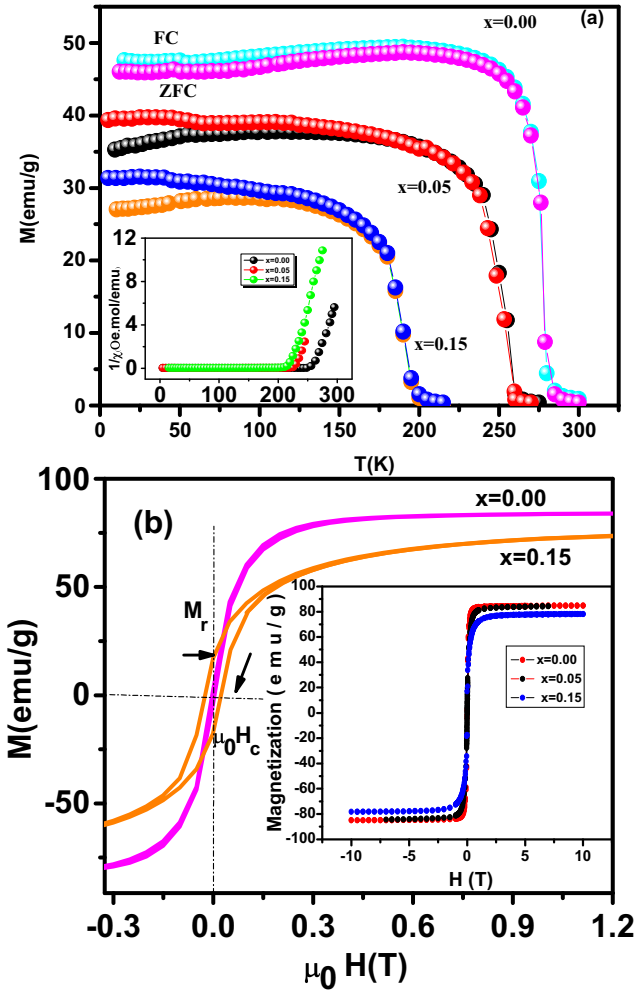

Fig. 3 Temperature dependences of the zero-field-cooled and field-cooled magnetization for LEBMFO samples, the inset show temperature dependent inverse susceptibility $\chi^{-1}(T)$ curves. **b** The hysteresis loops of LEBMFO samples ($x = 0.00$ and 0.15); the inset shows the field dependence of the magnetization plots taken at 5 K for all the samples in magnetic fields strengths of ±10 T

is generally related to a spin-glass or cluster-glass state. The discrepancy between ZFC and FC curves becomes proportionally larger with the doped content of Fe. In fact, the presence of cluster spin state in other doping systems has been extensively observed [35–37]. It is found that the Curie temperature T_C decreases with increasing x. The variance of T_C versus Fe concentration is tabulated in Table 3. One can note that T_C decreases swiftly when Fe content is increased. The number of Mn^{3+} is reduced appreciably and the ferromagnetic double-exchange interactions between Mn^{4+} and Mn^{3+} ions are weakened, while the antiferromagnetic interactions between Mn^{4+} and Fe^{3+} are reinforced.

From the determined C parameter, we have deduced the $\mu_{\text{eff}}^{\text{exp}}$ values. Assuming orbital momentum to be quenched in Er^{3+}, Mn^{3+}, Mn^{4+} and Fe^{3+}, the theoretical paramagnetic effective moment can be written as:

$\mu_{\text{eff}}^{\text{th}} = g\sqrt{J(J+1)}$, where $g = 1 + \frac{J(J+1)+S(S+1)-L(L+1)}{2J(J+1)}$ is the Landé factor, $J = |L - S|$ is the total moment, $L = \sum m_l$ is the orbital moment and $S = \sum m_S$ is the spin moment. The Svalues are 3/2 for Mn^{4+}, 2 for Mn^{3+}, 3/2 for Er^{3+} and 5/2 for Fe^{3+}. Thus, the theoretical values are $\mu_{\text{eff}}^{\text{th}}$ ($Mn^{3+} = 4.90\mu_B$), $\mu_{\text{eff}}^{\text{th}}$ ($Mn^{4+} = 3.87\mu_B$), $\mu_{\text{eff}}^{\text{th}}$ ($Er^{3+} = 9.58\mu_B$) and$\mu_{\text{eff}}^{\text{th}}$ ($Fe^{3+} = 5.92\mu_B$). The deduced $\mu_{\text{eff}}^{\text{exp}}$ value was then compared to the theoretical $\mu_{\text{eff}}^{\text{th}}$ calculated using the following relation:

$$(\mu_{\text{eff}}^{\text{th}})^2 = 0.05\,\mu_{\text{eff}}^2(Er^{3+}) + (0.67 - x)\mu_{\text{eff}}^2(Mn^{3+}) + 0.33\,\mu_{\text{eff}}^2(Mn^{4+}) + x\,\mu_{\text{eff}}^2(Fe^{3+}) \quad (5)$$

Furthermore, to better understand the effect of the substitution of Fe for Mn at low temperature, we calculated the values of saturation magnetic moment at $T = 5$ K considering the total spins of Mn^{3+}, Mn^{4+}, Er^{3+} and Fe^{3+} ions is given by

$$M_{\text{Sat}}(\text{cal}) = (M_{\text{Sat}\,Mn^{3+}})(n_{Mn^{3+}}) + (M_{\text{Sat}\,Mn^{4+}})(n_{Mn^{4+}}) + (M_{\text{Sat}\,Er^{3+}})(n_{Er^{3+}}) + (M_{\text{Sat}\,Fe^{3+}})(n_{Fe^{3+}}) \quad (6)$$

where $M_{\text{Sat}\,Mn^{3+}} = 4\mu_B$, $M_{\text{Sat}\,Mn^{4+}} = 3\mu_B$, $M_{\text{Sat}\,Er^{3+}} = 3\mu_B$ and $M_{\text{Sat}\,Fe^{3+}} = 5\mu_B$are the magnetic moments (the orbital contribution is neglected) and $n_{Mn^{3+}}$, $n_{Mn^{4+}}$, $n_{Er^{3+}}$ and $n_{Fe^{3+}}$ are the contents of the Mn^{3+}, Mn^{4+},

Table 3 Maximum entropy change $|\Delta S_M^{\max}|$ and relative cooling power (RCP), occurring at the Curie temperature (T_C) and under magnetic field 5 T for $La_{0.62}Er_{0.05}Ba_{0.33}Mn_{1-x}Fe_xO_3$ for ($x = 0.00$, 0.05 and 0.15) compounds, compared to several materials considered for magnetic refrigeration

Composition	T_C (K)	$\mu_0 H$ (T)	$\lvert\Delta S_M^{\max}\rvert$ (J/kg K)	RCP (J/kg)	References
$La_{0.62}Er_{0.05}Ba_{0.33}Mn_1O_3$	275	5	3.32	227.44	Our work
$La_{0.62}Er_{0.05}Ba_{0.33}Mn_{0.95}Fe_{0.05}O_3$	260	5	3.11	214.14	Our work
$La_{0.62}Er_{0.05}Ba_{0.33}Mn_{0.85}Fe_{0.15}O_3$	180	5	2.57	188.68	Our work
$La_{0.52}Dy_{0.15}Pb_{0.33}MnO_3$	290	5	3.51	246	[41]
Gd_5 (Si_2Ge_2)	275	5	18.5	535	[42]
$La_{0.8}Ba_{0.2}Mn_{0.9}Fe_{0.1}O_3$	193	5	2.62	211	[43]

Table 4 Magnetic parameters deduced from magnetization such as the moment effective experimental$\mu_{\text{eff}}^{\text{exp}}$, moment effective theoretical$\mu_{\text{eff}}^{\text{cal}}$, remnant magnetization M_r (emu/g), saturation magnetization (Ms), the coercive field $\mu_0 H_C$(T) and remnant ratio R = (Mr/Ms) of the system $La_{0.62}Er_{0.05}Ba_{0.33}Mn_{1-x}Fe_xO_3$ for ($x = 0.00$, 0.05 and 0.15) compounds

Samples	$\mu_{\text{eff}}^{\text{exp}}$	$\mu_{\text{eff}}^{\text{cal}}$	M_r(emu/g)	$\mu_0 H_C$(T)	Ms (emu/g)	R = (Mr/Ms)
$x = 0.00$	10.07	5.06	4.60	2.610^{-3}	84	0.054
$x = 0.05$	10.12	5.11	5.75	6.310^{-3}	80	0.071
$x = 0.15$	10.35	5.23	6.52	2.310^{-2}	75	0.240

Er^{3+} and Fe^{3+} ions respectively. The measured spontaneous magnetization at $T = 5$ K for =0.00, 0.05 and 0.15 compounds are found to be about 3.61, 3.22 and 2.45 μ_B, respectively, while the calculated values for full-spin alignment are 3.9, 3.655 and 3.165 μ_B, respectively. The spontaneous magnetization decreases with increasing Fe content. The difference between measured and calculated values should be explained by spin state at low temperature (Table 4). The effective magnetic moments are much higher than the theoretical value possibly because of the possible orbital charge fluctuations in contrast to charge orbital ordering in the parent compounds $La_{0.67}Ba_{0.33}MnO_3$.

The field dependence of magnetization at 5 K is plotted in the inset of Fig. 3b in magnetic fields strengths of ±10 T to complement the FC versus T data. The magnetization of all the samples nearly saturates above 1.5 T. On increasing Fe doping, the saturation magnetization (Ms) decreases. The hysteresis loops of $x = 0.00$ and $x = 0.15$ samples are plotted in Fig. 3b. The hysteresis in the M-H curve, along with the saturation, clearly confirms that we have a ferromagnetic state at low temperatures. It can be clearly seen that both the coercive field ($\mu_0 H_c$) and the remanence magnetization (M_r) increase systematically with the increase of Fe doping. The coercive field has increased by more than an order of magnitude from 2.610^{-3} T for the undoped ($x = 0.00$) sample to nearly 2.310^{-2} T for $x = 0.15$ Fe-doped sample. Markovich et al. [38] suggested that suppression of the FM phase results in decrease of magnetization and increase of H_C. In this case, the interfacial spins between FM and AFM regions tend to rotate with the FM domains. These spins experience an increasing rotational drag due to the AFM domains, leading to broadening of the hysteresis loops.

Figure 4 shows the variation of remanence magnetization (Mr) and saturation magnetization (Ms) with Fe^{3+} substitution. The force required for demagnetization of a sample is termed as remanence magnetization and is one of the important parameters to be considered in recording media industry. Remanence is a structure sensitive parameter. For the present system, the values of remanence varied in the range of 4.60–18.20 emu/g. The remnant ratio R = Mr/Ms is a characteristic parameter of the material. It is an indication of the ease with which the direction of magnetization reorients to the nearest easy axis of magnetization direction after the magnetic field is removed. Within this framework, it is desirable to have higher remnant ratio for magnetic recording and memory devices [39]. The values of R in the present case varied for one magnitude of order and the values are found 0.054, 0.071 and 0.240 for $x = 0.00$, 0.05 and 0.15, respectively. The values show increasing trend with Fe^{3+} substitution.

In Fig. 5, we show magnetization isotherms, M (μ_0H), for $x = 0.00$ and $x = 0.15$ samples taken over a certain temperature range around their respective Curie temperatures. The data were taken at 5-K intervals close to T_C and away from T_C. We have found a soft ferromagnetic behaviour at all temperatures in Fe-doped compounds. The same result is shown during Fe doping at Mn site in the same parent compound [40]. Banerjee [41] suggested an experimental criterion which allows the determination of the nature of the magnetic transition (first or second order). It consists in observing the slope of the isotherms plots M^2 versus $\mu_0 H/M$ applying a regular approach, the straight line was constructed simply extrapolating the high magnetization parts of the curves for each studied temperature. A positive or negative slope indicates a second- or a first-order transition, respectively. Figure 6a, b shows the isotherm plots M^2 versus$\mu_0 H/M$ above and below

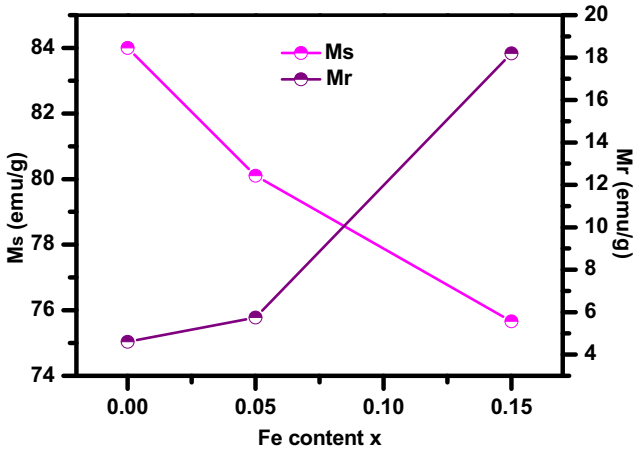

Fig. 4 Variation of saturation magnetization (Ms) and remanence magnetization (Mr) with Fe content

T_C for $x = 0.00$ and $x = 0.15$ samples, respectively. These samples show positive slopes in the complete M^2 range, indicating that the system exhibits a second-order ferromagnetic to paramagnetic phase transition.

3.3 Magnetocaloric Behaviours

The magnetocaloric effect is an intrinsic property of magnetic materials. It is the response of the material to the application or removal of magnetic field, which is maximized when the material is near its magnetic ordering temperature (Curie temperature T_C).

From the Maxell's thermodynamic equation, the magnetic entropy change as the field is varied from $\mu_0 H = 0$ to $\mu_0 H = \mu_0 H_{\max}$. Can be written as:

$$\Delta S_M = \int_0^{\mu_0 H_{\max}} \left(\frac{\partial M}{\partial T}\right)_H dH \tag{7}$$

The numerical evaluation of this integral can be approximated to give

$$\Delta S_M = \sum \left[\left(M_i(T_i, H) - M_{i+1}(T_{i+1}, H)\right) / (T_i - T_{i+1}) \right] \Delta H \tag{8}$$

where M_i and M_{i+1} are the magnetization values measured at temperatures T_i and T_{i+1}, respectively, and $\Delta\mu_0 H$ represents the field variation from $\mu_0 H = 0$ until $\mu_0 H_{\max}$.

The $-\Delta S_M$ values for different $\Delta_{\mu 0} H$ as a function of temperature are presented in Fig. 7 determined under an applied magnetic field equal 5 T. The $-\Delta S_M$ is positive in the entire temperature range for all the samples. The magnetic entropy for $\Delta_{\mu 0} H = 5$ T increases with lowering temperature from $T \ll T_C$, others goes through a maximum around T_C and then decreases for $T \gg T_C$. The magnitude of the peak increases with increasing value of $\Delta_{\mu 0} H$ for each composition but the peak position is nearly unaffected because of the second-order nature of the ferromagnetic

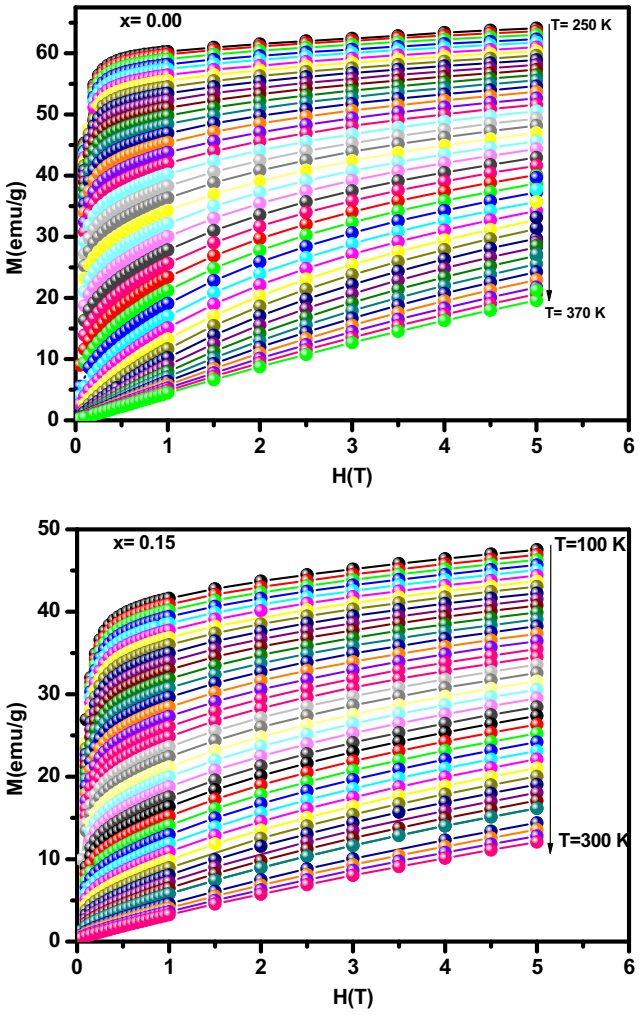

Fig. 5 Isothermal magnetization as a function of applied field for $La_{0.62}Er_{0.05}Ba_{0.33}Mn_{1-x}Fe_xO_3$ for ($x = 0.00$ and 0.15)

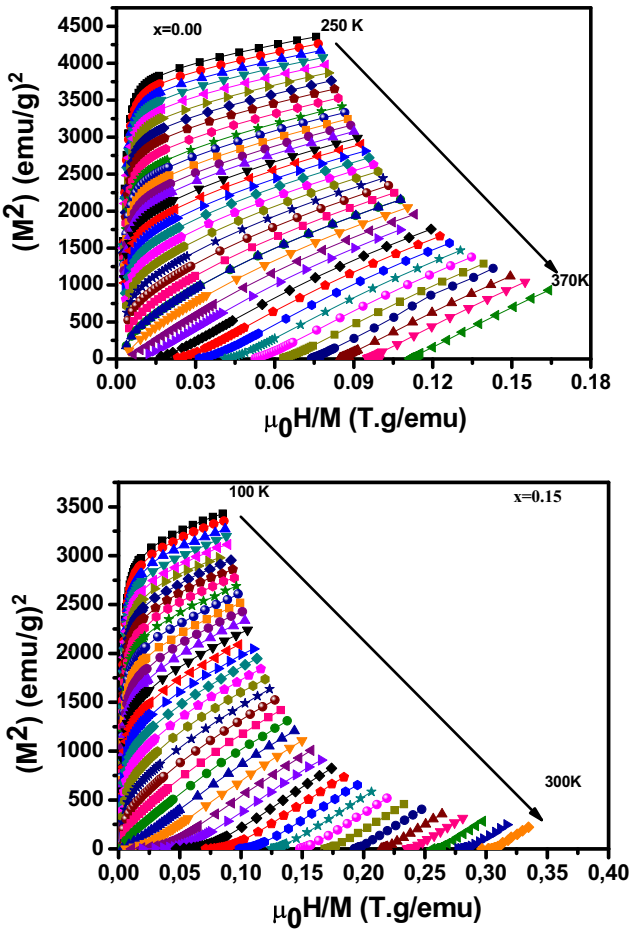

Fig. 6 the Arott plots of M^2 versus $\mu_0 H/M$ at various temperatures for $La_{0.62}Er_{0.05}Ba_{0.33}Mn_{1-x}Fe_xO_3$ for ($x = 0.00$ and 0.15) samples

transition in these compounds. Furthermore, the value of the peak decreases with increasing Fe content around T_C from $-\Delta S_M = 3.32$ J/kg K for $= 0.00$ to 2.57 J/kg K for $x = 0.15$. Thus, it reduces the maximum ΔS_M value. As it is well known, the double-exchange interaction controls the close relationship between the structure and the magnetic properties in this kind of materials. The partial substitution of Mn^{3+} by Fe^{3+}, causes a decrease of the Mn^{3+}/Mn^{4+} ratio and greatly weakens the double-exchange interaction of Mn^{3+}–O–Mn^{4+} and replaced by antiferromagnetic Mn–O–Fe interactions, which lead to a progressive dilution of ferromagnetism [29].

For comparison, we have listed in Table 3 the data of various magnetic materials that could be used as magnetic refrigerants. Although the values of $\left|\Delta S_M^{\max}\right|$are smaller than the most conspicuous MC material Gd_5 (Si_2Ge_2), these perovskite manganites are easy to manufacture and exhibit higher A- or B-site doping. Consequently, a large magnetic entropy change can be tuned from low temperature to near- or above-room temperature which is beneficial for operating magnetic refrigeration at various temperature ranges.

On the other hand, the specific heat can be calculated from the field dependence of the external magnetic entropy from zero to $\mu_0 H_{\max}$ by the following equation [44]:

$$\Delta C_P\,(T, \mu_0 H) = C_P(T, \mu_0 H) - C_P(T, 0) = -T\,\frac{\partial\,(\Delta S_M\,(T, \mu_0 H))}{\partial T} \tag{9}$$

From this formula, $\Delta C_P(T,\mu_{\ 0}H)$ of $La_{0.62}Er_{0.05}Ba_{0.33}Mn_{1-x}Fe_xO_3$ for ($x = 0.05$) sample versus temperature at different magnetic fields is shown in Fig. 8. The value of ΔC_P suddenly changes from positive to negative around Curie temperature (T_C) and rapidly decreases with decreasing temperature.

From the results of the magnetic entropy change, it was determined that the relative cooling power (RCP), a parameter used to evaluate the refrigeration capacity of a magnetic refrigerant [45]. The RCP value is obtained fromRCP $= \Delta S_M \times \partial T_{\mathrm{FWHM}}$. We found that RCP = 227.445, 214.148 and 188.684 J/kg for $x = 0.00$, 0.05 and 0.15, respectively. It is important to note that even though

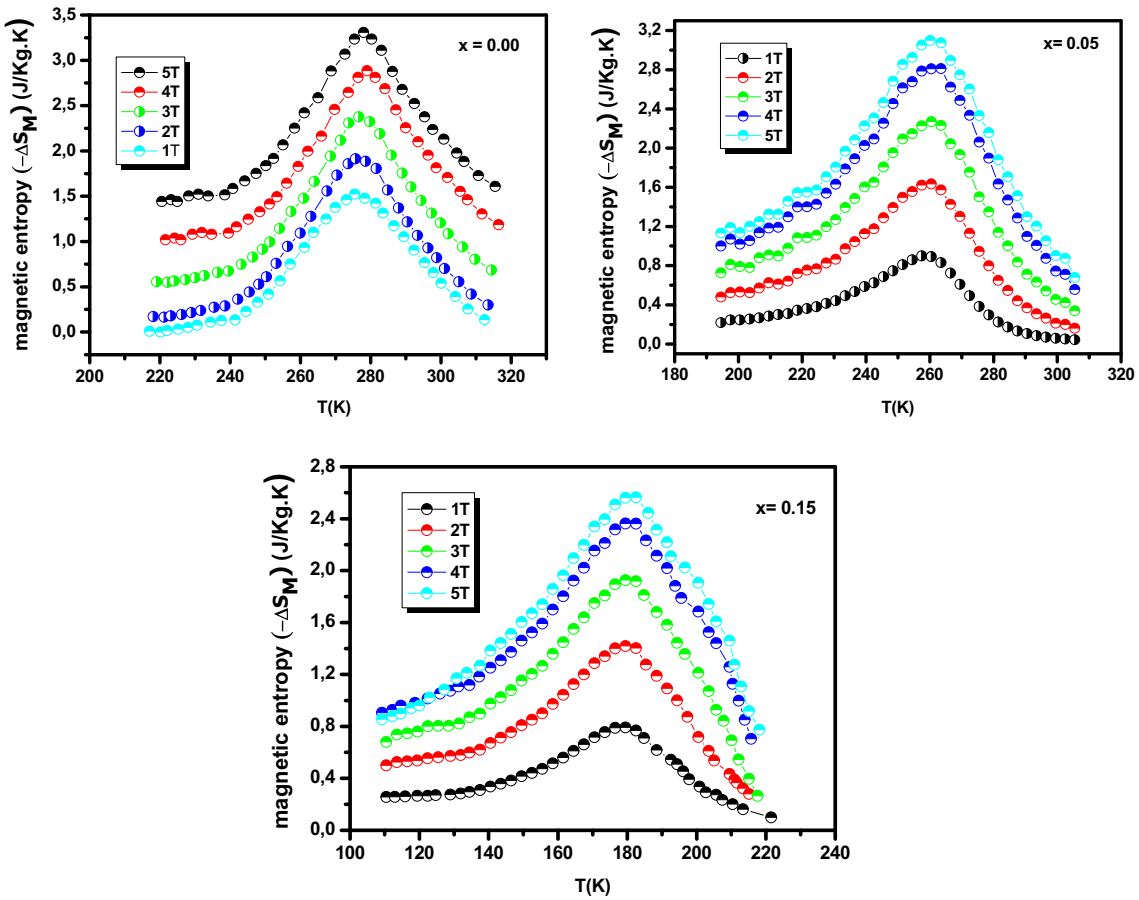

Fig. 7 Temperature dependence of the magnetic entropy change ($-\Delta S_M$) at different applied magnetic field change interval for $La_{0.62}Er_{0.05}Ba_{0.33}Mn_{1-x}Fe_xO_3$ for ($x = 0.00$, 0.05 and 0.15) samples

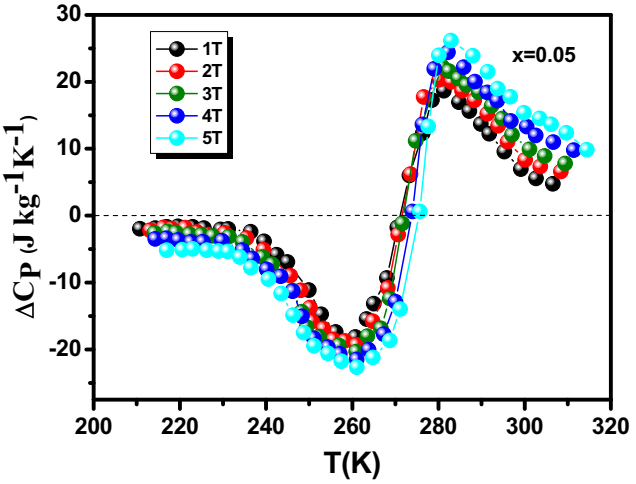

Fig. 8 Change of specific heat of the sample as a function of temperature at different magnetic fields for $x = 0.05$

the peak value of ΔS_M decreases the RCP value decreases with increasing Fe doping. These values are higher than those of $La_{0.67}Ba_{0.33}MnO_3$ (RCP = 161 J/kg at $T = T_C$) [46]. Since the RCP factor represents a good way for comparing magnetocaloric materials, our compounds can be considered as potential candidates thanks to their high RCP values compared with available refrigerant materials.

We can use ΔS_M^{max} and $\mu_0 H$ to confirm that our materials exhibit a second-order transition [47, 48]. The magnetic materials with a second-order transition generally obey $\Delta S_M^{max} = -kM_S(0)\, h^{2/3} - S(0,0)$, where h is the reduced field just around $T_C[h = (\mu_0\mu_B H)/(k_B T_C)]$, k is a constant, Ms (0) is the saturation magnetization at low temperatures and S (0.0) is the reference parameter, which may not be equal to zero [48] Fig. 9 shows the linear dependence of ΔS_M^{max} versus $h^{2/3}$ which implies the secondorder transition in $La_{0.62}Er_{0.05}Ba_{0.33}Mn_{1-x}Fe_xO_3$ for ($x = 0.00$, 0.05 and 0.15). The fact that ΔS_M^{max} is estimated at T_C and in fields larger than the critical field required for the metamagnetic transition justifies the conclusion about the second-order transition.

3.4 Correlation Between Critical Exponents and Magnetocaloric Effect

Numerous works have focused on the dependence of the magnetic entropy change (ΔS_M) of manganites at the FM-PM transition on T_C. According to Oesterreicher et al. [49], the magnetic field dependence on the magnetic entropy changeΔS_M at a temperature T for materials obeying a second-order phase transition follows an exponent power law of the type [50]: $\Delta S_M = b(\mu_0 H)^n$:

$$n = \frac{d\ln \Delta S_M}{d\ln H} = -\frac{\mu_0 H}{\Delta S_M}\left(\frac{\partial M}{\partial T}\right)_H \tag{10}$$

where b is a constant and the exponent n depends on the values of field and temperature. By fitting the data of ΔS_M versus $\mu_0 H$ to (10), we obtain the value of n as a function of temperature at different magnetic fields for example $x = 0.05$, as depicted in Fig. 10. From this figure, the exponent n is close to 1 in the FM regime and increases to 2 in the PM regime. The exponent n exhibits a moderate increase with decreasing temperature and takes extreme values around Curie temperature of the existing phase, then sharply increases with increasing temperature. In a mean field approach, the value of n at Curie temperature is predicted to be 2/3 [50]. It is well known in manganites that the exponent is roughly field-independent and approaches approximate values of 1 and 2, far below and above the transition temperature, respectively [51]. Then, the values

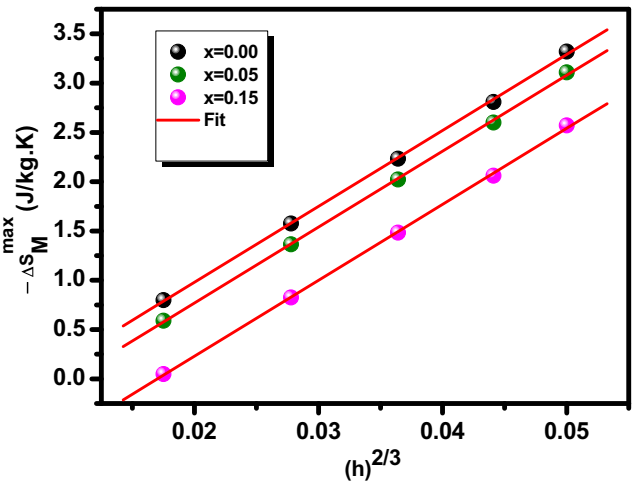

Fig. 9 Temperature dependence of magnetic entropy change $-\Delta_M^{max}$ versus $h^{2/3}$ for $La_{0.62}Er_{0.05}Ba_{0.33}Mn_{1-x}Fe_xO_3$ for ($x = 0.00$ and 0.15) samples

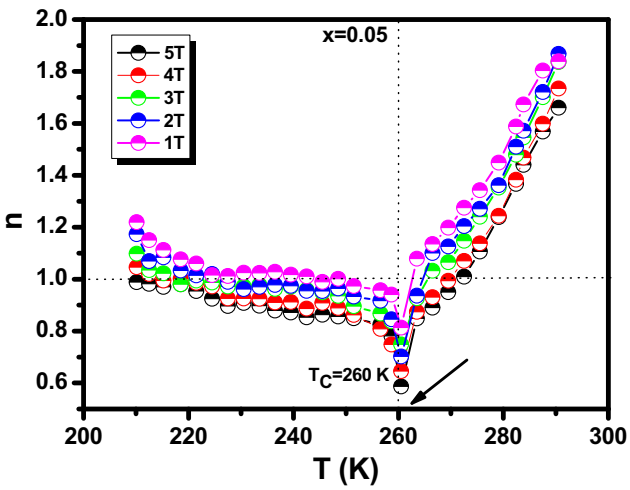

Fig. 10 Temperature dependence of the local exponent n for $x = 0.05$ at different magnetic fields

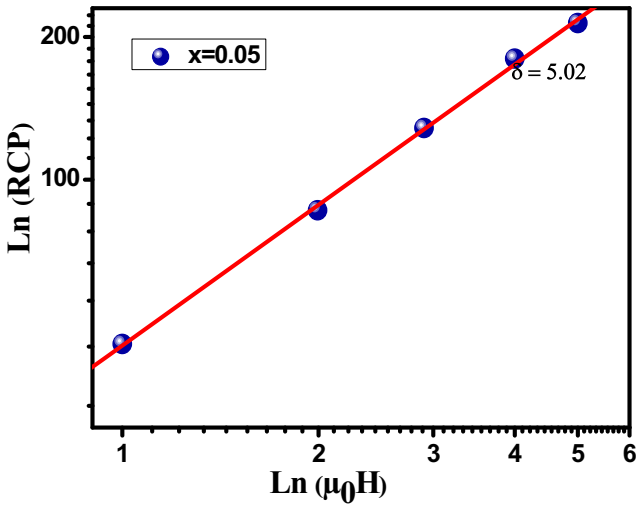

Fig. 11 Variation of Ln (RCP) as function of applied magnetic field for $x = 0.05$ sample. Red line indicates the linear fit for d calculation

of n around T_C are 0.561, 0.584 and 0.613 for $x = 0.00$, 0.05 and 0.15, respectively, which confirms not only the invalidity of the mean field model in the description of our materials at near the transition temperature for our samples but also the probability of 3D Ising model and 3D Heisenberg model to describe our material. These values are similar to those obtained for soft magnetic materials containing rare earth metals [52, 53].

The field dependence of RCP, for our samples is also analysed. It can be expressed as a power law by taking account of the field dependence of entropy change ΔS_M and reference temperature into consideration [54].

$$\mathrm{RCP} \propto \mu_0 H^{1+\frac{1}{\delta}} \tag{11}$$

where δ is the critical exponent of the magnetic transition. Field dependence of RCP is displayed in Fig. 11 for $x = 0.05$. The obtained values of δ are 3.2 (3), 3.34 (2), and 2.82 (3) for $x = 0.00$, 0.05 and 0.15, respectively. In the particular case of $T = T_C$ or at the temperature when the entropy is maximal, the exponent (n) becomes an independent field [55]. In this case,

$$n\,(T_C) = 1 + \frac{\beta - 1}{\beta + \gamma} \tag{12}$$

Table 5 Critical β and γ parameters calculated from n and δ

Samples	Number	δ	β	γ	T_C (K)
$x = 0.00$	0.561	4.98	0.313	1.251	275
$x = 0.05$	0.584	5.02	0.323	1.304	260
$x = 0.15$	0.613	4.85	0.347	1.340	180

where β and γ are the critical exponents [56]. With $\beta\delta = (\beta + \gamma)$ [56], the relation (7) can be written as:

$$n\,(T_C) = 1 + \frac{1}{\delta}\left(1 - \frac{1}{\beta}\right) \tag{13}$$

From the values of n and δ, the critical parameters β and γ are deduced for each compound using (12) and (13) (Table 5).

4 Conclusion

In conclusion, we have reported detailed investigations of morphological, magnetic and magnetocaloric properties of $La_{0.62}Er_{0.05}Ba_{0.33}Mn_{1-x}Fe_xO_3$ for ($x = 0.00$, 0.05 and 0.15). The samples were prepared by the standard ceramic process. T_C decreases swiftly by substituting Fe for Mn. Moreover, there is cluster spin state in all investigated samples. It is also found that the entropy change and the relative cooling power during the phase transition are reduced with the increase in Fe. These observations indicate that the existence of Fe has the effect of weakening ferromagnetism in the LEBMFO perovskite.

References

1. Zhang, D., Klabunde, K.J., Sorensen, C.M., Hadjipanayis, G.C.: Phys. Rev. B. **58**, 14167 (2006)
2. Kaman, O., Pollert, E., Veverka, P., Ververka, M., Hadova, E., Knizek, K., Marysko, M., Kaspar, P., Klementova, M., Grunwaldova, V., Vasseur, S., Epherre, R., Mornet, S., Goglio, G., Duguet, E.: Nanotechnology **20**, 275610 (2009)
3. Chono, S., Li, S.-D., Conwell, C.C., Huang, L.: J. Control. Release. **131**, 64 (2008)
4. Hu, X.-J., Liu, J.-K., Mu, Y.: J. Mater. Lett. **62**, 3824 (2008)
5. Liu, J., Zhao, Z., Wang, J., Xu, C., Duan, A., Jiang, G., Yang, Q.: Appl. Catal. B. **84**, 185 (2008)
6. Abassi, M., Dhahri, N., Dhahri, J., Hlil, E.K.: J. Physica B: Condens. Matter. **449**, 138–143 (2014)
7. Gdaiem, M.A., Abassi, M., Dhahri, J., Hlil, E.K.: J. Alloys Compd. **646**, 1068–1074 (2015)
8. Thaljaoui, R., Boujelben, W., Pękaa, M., Pękaa, K., Antonowicz, J., Fagnard, J.-F., vanderbemdend, Ph.., Dąbrowska, S..: J. Mucha. J. Alloys Comp. **611**, 427–432 (2014)
9. Jin, S., Tiefel, T.H., McCormack, M., Fastnacht, R.A., Ramesh, R., Chen, L.H.J.: Science. **264**, 413–415 (1994)
10. Khazeni, K., Jia, Y.X., Lu, L., Crespi, V.H., Cohen, M.L., Zettl, A.: Phys. Rev. Lett. **76**, 295–298 (1996)
11. Giri, S.K., Dasgupta, P., Poddar, A., Nigam, A.K., Nath, T.K.: Nath. J. Alloys Compd. **582**, 609–616 (2014)

12. Balagurov, A.M., Bushmeleva, S.N., Pomjakushin, V.Yu., Sheptyakov, D.V., Amelichev, V.A., Gorbenko, O.Yu., Kaul, A.R., Gan'shina, E.A., Perkins, N.B.: Phys. Rev. B **70**, 014427 (2004)
13. Granado, E., Huang, Q., Lynn, J.W., Gopalakrishnan, J., Ramesha, K.: Phys. Rev. B **70**, 214416 (2004)
14. Phan, M.H., Yu, S.C.: J. Magn. Magn. Mater. **308**, 325–340 (2007)
15. Dincer, I., Yüzüak, E., Durak, G., Elerman, Y.: J. Alloys Compd. **588**, 332–336 (2014)
16. Zhang, Y., Yang, B.: J. Alloys Compd. **610**, 540–543 (2014)
17. Bohigas, X., Tejada, J., Del Barco, E., Zhang, X.X., Sales, M.: Appl. Phys. Lett. **73**, 390–392 (1998)
18. Bruck, E.: J. Phys. D: Appl. Phys. **38**, 381–391 (2005)
19. Takeya, H., Pecharsky, V.K., Gschneidner, K.A. Jr., Morman, J.O.: Appl. Phys. Lett. **64**, 2739–2741 (1994)
20. Mahjoub, S., Baazaoui, M., M'nassri, R., Rahmouni, H., Boudjada, N.C., Oumezzine, M.: J. Alloys Comp. **608**, 191–196 (2014)
21. Podmiljsak, B., Kim, J.-H., McGuiness, P.J., Kobe, S.: J. alloys Compd. **591**, 29–33 (2014)
22. Sun, J.R., Rao, G.H., Shen, B.G., Wong, H.K.: J. Appl. Phys. Lett. **73**, 2998–3000 (1998)
23. Ghosh, K., Ogale, S.B., Ramesh, R., Greene, R.L., Venkatesan, T., Gapchup, K.M., Bathe, R., Patil, S.I.: Phys. Rev. B **59**, 533–537 (1999)
24. Huang, Y., Liao, C., Wang, Z., Li, X., Yan, C., Sun, J., Shen, B.: Phys. Rev. B 65 (2002)
25. Oumezzine, E., Hcini, S., Hlil, E.-K., Dhahri, E., Oumezzine, M.: J. alloys Compd. **615**, 553–560 (2014)
26. Simopoulos, A., Pissas, M., Kallias, G., Devlin, E., Moutis, N., Panagiotopoulos, I., Niarchos, D., Christides, C.: Phys. Rev. B. **59**, 1263–1271 (1999)
27. Lenug, L.K., Morrish, A.H., Evans, B.J.: Phys. Rev. B. **13**, 4069–4078 (1976)
28. Blanco, J.J., Insausti, M., Muro, I., Lezama, L., Rojo, T.: J. Solid State Chem. **179**, 623–631 (2006)
29. Abassi, M., Mohamed, Za., Dhahri, J., Hlil, E.K.: J. Alloys Compd. **639**, 197–202 (2015)
30. Li, Z.Q., Jiang, E.Y., Ren, S.W., Hou, D.L., Wu, P., Bai, H.L.: J. Phys. Status Solidi. **A195**(2), 429–433 (2003)
31. Abassi, M., Dhahri, N., Tahri, T., Dhahri, J., Taibi, K., Hlil, E.K.: J. Ceram. Inter. **41**, 1847–1855 (2015)
32. Suryanarayana, C., Norton, M.G.: p. 213. Press, New York and London (1988)
33. Rao, K.S., Tilak, B., Rajula, K.Ch.V., Swathi, A., Workinech, H.: J. Alloys Comp. **509**, 7121–7129 (2011)
34. Ying, Y., Fan, J., Pi, L., Qu, Z., Wang, W., Hong, B., Tan, S., Zhang, Y.: J. Phys. Rev. B **74**, 144433 (2006)
35. Cai, J.W., Wang, C., Shen, B.G., Zhao, J.G., Zhan, W.S.: J. Appl. Phys. Lett. **71**, 1727 (1997)
36. Ritter, C., Oseroff, S., Cheong, S.W.: J. Phys. Rev. B. **56**, 8902 (1997)
37. Baazaoui, M., Zemni, S., Boudard, M., Rahmouni, H., Gasmi, A., Selmi, A., Oumezzine, M.: J. Nanoelectron. Mater. **3**, 23–26 (2010)
38. Markovich, V., Fita, I., Puzniak, R., Martin, C., Wisniewski, A., Yaicle, C., Maignan, A., Gorodetsky, G.: J. Magn. Magn. Mater. **316**, 636 (2007)
39. Shirsath, S.E., Jadhav, S.S., Toksha, B.G., Patange, S.M., Jadhav, K.M.: J. Appl. Phys. **110**, 013914 (2011)
40. Cherif, R., Hlil, E.K., Ellouze, M., Elhalouani, F., Obbade, S.: J. Solid State. Chem. **215**, 271–276 (2014)
41. Mohamed, Za., Tka, E., Dhahri, J., Hlil, E.K.: J. Alloys Compd. **619**, 520–526 (2015)
42. Pekala, M., Drozd, V.: J. Non-Cryst. Solids **354**, 5308–5314 (2008)
43. Ghodhbane, S., Dhahri, A., Dhahri, N., Hlil, E.K., Dhahri, J.: J. Alloys Comp. **550**, 358–364 (2013)
44. Dhahri, Ah., Jemmali, M., Dhahri, E., Valente, M.A.: J. Alloys Compd. **638**, 221–227 (2015)
45. Mohamed, Za., Abassi, M., Tka, E., Dhahri, J., Hlil, E.K.: J. Alloys Compd. **646**, 23–31 (2015)
46. Oumezzine, M., Zemni, S., Pena, O.: J. Alloys Compd. **508**, 292–296 (2010)
47. Dong, Q.Y., Zhang, H.W., Shen, J.L., Sun, J.R., Shen, B.G.: J. Magn. Magn. Mater. **319**, 56–59 (2007)
48. Franco, V., Conde, A., Pecharsky, V., Gschneidner, K.A.: J. Euro Phys. Lett. **79**, 47009–47011 (2007)
49. Oesterreicher, H., Parker, F.T.: J. Appl. Phys. **55**, 4334–4338 (1984)
50. Shen, T.D., Schwarz, R.B., Coulter, J.Y., Thompson, J.D.: J. Appl. Phys. **91**, 5240–5245 (2002)
51. Pekala, M.: J. Appl. Phys. **108**, 113913–113916 (2010)
52. Franco, V., Conde, C.F., Blazquez, J.S., Conde, A., Svec, P., Janičkovic, D., Kiss, L.F.: J. Appl. Phys. **101**, 093903 (2007)
53. Abassi, M., Dhahri, N., Dhahri, J., Taibi, K., Hlil, E.K.: J. Rare Earths **33**, 263–270 (2015)
54. Franco, V., Conde, A.: Int. J. Refrig. **33**, 465 (2010)
55. Franco, V., Conde, A., Kuz'min, M.D., Romero-Enrique, J.M.: J. Appl. Phys. **105**, 917 (2009)
56. Widom, B.: J. Chem. Phys. **43**, 3898 (1965)